Chiral geometry in multiple chiral doublet bands[*]

Hao Zhang (张灏)   Qibo Chen (陈启博)[1)]

State Key Laboratory of Nuclear Physics and Technology, School of Physics, Peking University, Beijing 100871, China

Abstract: The chiral geometry of multiple chiral doublet bands with identical configuration is discussed for different triaxial deformation parameters γ in the particle rotor model with $\pi h_{11/2} \otimes \nu h_{11/2}^{-1}$. The energy spectra, electromagnetic transition probabilities $B(M1)$ and $B(E2)$, angular momenta, and K-distributions are studied. It is demonstrated that the chirality still remains not only in the yrast and yrare bands, but also in the two higher excited bands when γ deviates from $30°$. The chiral geometry relies significantly on γ, and the chiral geometry of the two higher excited partner bands is not as good as that of the yrast and yrare doublet bands.

Keywords: multiple chiral doublet bands, particle rotor model, triaxial deformation parameter, chiral geometry

PACS: 21.60.Ev, 21.10.Re, 23.20.Lv   **DOI:** 10.1088/1674-1137/40/2/024102

1   Introduction

The phenomenon of spontaneous chiral symmetry breaking has attracted significant attention in recent years. Since the chirality of a triaxial atomic nucleus was first predicted in 1997 by Frauendorf and Meng [1] and identified in 2001 by Starosta et al [2], many achievements have been made.

Experimentally, more than 30 candidate chiral nuclei have been found in the $A \sim 80$ [3], 100 [4–19], 130 [2, 20–45] and 190 [46–50] mass regions. For more details see, e.g., Refs. [51–56].

Theoretically, many approaches have been developed to investigate nuclear chirality, such as the particle rotor model (PRM) [1, 24, 29, 57–76], the tilted axis cranking model (TAC) [1, 77–79], the tilted axis cranking plus random phase approximation (TAC+RPA) [38, 80], the interacting boson fermion–fermion model (IBFFM) [36, 39, 81–84], the pair truncated shell model (PTSM) [85–87], and the projected shell model (PSM) [88]. Recently, based on the TAC, a microscopical collective Hamiltonian was constructed and applied to the unified description of chiral vibration and rotation [89].

Due to the successful description of nuclear global properties and exotic phenomena [90–92], covariant density function theory (CDFT) has been introduced to investigate the triaxial deformation of chiral nuclei with various configurations. Based on adiabatic and configuration-fixed constrained triaxial CDFT, the pos-

sible existence of multiple chiral doublets (MχD), i.e., more than one pair of chiral doublet bands in one single nucleus, was proposed for odd–odd nucleus ^{106}Rh [93]. In fact, the MχD phenomena has been experimentally observed in ^{105}Rh separately by Alcántara-Núñez et al [6] and Timár et al [7] though the acronym MχD was not introduced. The observation of the two doublets was substantiated by TAC calculations demonstrating the existence of chiral solution for the two configurations $\pi g_{9/2}^{-1} \otimes \nu h_{11/2}(g_{7/2}, d_{5/2})$ [6] and $\pi g_{9/2}^{-1} \otimes \nu h_{11/2}^2$ [7]. More MχD nuclei were predicted in the other rhodium isotopes [94–96]. In Ref. [96], the existence of the MχD phenomena in ^{105}Rh is again supported by the constrained triaxial CDFT calculations. Later on, the experimental evidence for the predicted MχD was first reported simultaneously in ^{133}Ce [97], and also possibly in ^{107}Ag [98].

In contrast to MχD in which different partner bands are of distinct triaxial deformations and configurations, the MχD phenomenon is also expected with identical configurations, i.e., not only the yrast and yrare bands but also higher excited bands might be chiral partner bands [99–101]. The energy spectra of MχD are first presented with rigid and soft cores [99]. Then the chiral geometry of MχD was examined for the configuration $\pi h_{11/2} \otimes \nu h_{11/2}^{-1}$ with constant and spin-dependent variable moments of inertia at $\gamma = 30°$ [100]. It was confirmed that the MχD can indeed exist in identical configurations. The chiral geometry of MχD has been further examined for the configuration $\pi g_{9/2} \otimes \nu h_{11/2}^{-1}$ at

$\gamma = 30°, 20°$ [101]. Very recently, the evidence of this type of MχD was first observed in ^{103}Rh [102]. This observation shows that the chiral geometry in nuclei can be robust against the increase of the intrinsic excitation energy.

As mentioned previously, MχD with identical configurations have been investigated for the ideal chiral system, i.e., one $h_{11/2}$ proton particle and one $h_{11/2}$ neutron hole coupled to a rigid rotor with triaxial deformation $\gamma = 30°$ [100], and its chiral geometry has been examined by analyzing the evolution of angular momentum. Thus, it is intriguing and necessary to study the chiral geometry of MχD with identical configuration in more general cases where γ deviates from $30°$.

In this paper, the physical observables and chiral geometry of the MχD with identical configuration are discussed for different triaxial parameters γ with $\pi h_{11/2} \otimes \nu h_{11/2}^{-1}$ in the PRM. The paper is organized as follows. In Section 2, the theoretical framework of the PRM is briefly introduced. The numerical details are presented in Section 3. In Section 4, the obtained energy spectra, electromagnetic transition probabilities B(M1) and B(E2), angular momenta, as well as K-distributions are shown and discussed in detail. Finally, a summary is given in Section 5.

2 Theoretical framework

The detailed theoretical framework for the PRM can be found in Refs. [1, 57, 60, 66, 73]. In this section, for completeness, some key formulas are presented. The Hamiltonian of the PRM is

$$\hat{H}_{\mathrm{PRM}} = \hat{H}_{\mathrm{coll}} + \hat{H}_{\mathrm{intr}}, \tag{1}$$

in which the collective Hamiltonian is

$$\hat{H}_{\mathrm{coll}} = \sum_k \frac{\hat{R}_k^2}{2\mathcal{J}_k} = \sum_k \frac{(\hat{I}_k - \hat{J}_k)^2}{2\mathcal{J}_k}, \tag{2}$$

where the indices $k = 1, 2, 3$ refer to the principal axes in the body-fixed frame of reference, and $\hat{I}_k$, $\hat{R}_k$, $\hat{J}_k$ represent the angular momenta of the total nucleus, core, and valence nucleons. The moments of inertia along the three principal axes depend on the triaxial deformation parameter γ, and $\mathcal{J}_k = \mathcal{J}_0 \sin^2(\gamma - 2\pi k/3)$ [103]. The Hamiltonian of the intrinsic nucleon $\hat{H}_{\mathrm{intr}}$ takes the single-j shell Hamiltonian [1, 57, 60, 66, 73].

The PRM eigenstates are obtained by diagonalizing the Hamiltonian (1) with a strong coupling basis [57]

$$|IM\alpha\rangle = \sqrt{\frac{1}{2(1+\delta_{K0})}} \left\{ \sum_{K,k_{\mathrm{p}},k_{\mathrm{n}}} C_{k_{\mathrm{p}}k_{\mathrm{n}}}^{IK\alpha} \Big[|IMKk_{\mathrm{p}}k_{\mathrm{n}}\alpha\rangle \right. $$
$$\left. + (-1)^{I-j_{\mathrm{p}}-j_{\mathrm{n}}} |IM-K-k_{\mathrm{p}}-k_{\mathrm{n}}\alpha\rangle \Big] \right\}, \tag{3}$$

where $|IMK\rangle$ is the Wigner D function, $|k_{\mathrm{p}}k_{\mathrm{n}}\rangle$ is the product of the proton and neutron states, and $C_{k_{\mathrm{p}}k_{\mathrm{n}}}^{IK\alpha}$ is the expansion coefficient. The angular momentum projections onto the quantization axis (3-) in the intrinsic frame and the z axis in the laboratory frame are denoted by K and M, respectively. The other quantum numbers are denoted by α.

With the obtained eigenstates, the reduced transition probability can be calculated according to

$$B(\sigma\lambda, I'\alpha' \to I\alpha) = \sum_{M'M} \left| \langle f, IM\alpha | \hat{T}_{\lambda\nu} | i, I'M'\alpha' \rangle \right|^2, \tag{4}$$

where $\sigma = E$ or M indicates electric or magnetic transition, respectively, and λ is the rank of the electric or magnetic transition operator from initial state $|i\rangle$ to final state $|f\rangle$. Thus, for the reduced electric quadrupole transition probability

$$B(\mathrm{E2}, I'\alpha' \to I\alpha)$$
$$= \frac{5Q_0^2}{16\pi} \left| \sum_{K,K'}^{k_{\mathrm{p}},k_{\mathrm{n}}} C_{k_{\mathrm{p}}k_{\mathrm{n}}}^{IK\alpha} C_{k_{\mathrm{p}}'k_{\mathrm{n}}'}^{I'K'\alpha'} \Big[\cos\gamma \langle IK20|I'K'\rangle \right.$$
$$\left. - \frac{\sin\gamma}{\sqrt{2}} \big(\langle IK22|I'K'\rangle + \langle IK2-2|I'K'\rangle \big) \Big] \right|^2, \tag{5}$$

and for the reduced magnetic dipole transition probability

$$B(M1, I'\alpha' \to I\alpha)$$
$$= \frac{3}{16\pi} \left| \sum_{\mu,k_{\mathrm{p}},k_{\mathrm{n}},k_{\mathrm{p}}',k_{\mathrm{n}}'} \frac{1}{(1+\delta_{K'0})} \frac{1}{(1+\delta_{K0})} \right.$$
$$\times C_{k_{\mathrm{p}}k_{\mathrm{n}}}^{IK\alpha} C_{k_{\mathrm{p}}'k_{\mathrm{n}}'}^{I'K'\alpha'} \Big[\langle IK1\mu|I'K'\rangle \langle k_{\mathrm{p}}'k_{\mathrm{n}}'| [(g_{\mathrm{p}}-g_{\mathrm{R}})j_{\mathrm{p}\mu}$$
$$+ (g_{\mathrm{n}}-g_{\mathrm{R}})j_{\mathrm{n}\mu}] |k_{\mathrm{p}}k_{\mathrm{n}}\rangle$$
$$+ (-1)^{I-j_{\mathrm{p}}-j_{\mathrm{n}}} \langle I-K1\mu|I'K'\rangle \langle k_{\mathrm{p}}'k_{\mathrm{n}}'| [(g_{\mathrm{p}}-g_{\mathrm{R}})j_{\mathrm{p}\mu}$$
$$\left. + (g_{\mathrm{n}}-g_{\mathrm{R}})j_{\mathrm{n}\mu}] |-k_{\mathrm{p}}-k_{\mathrm{n}}\rangle \Big] + \mathrm{sign} \right|^2. \tag{6}$$

Here, Q_0 is the intrinsic quadrupole moment; g_{R}, g_{p}, and g_{n} are the gyromagnetic ratios of rotor, proton, and neutron, respectively.

3 Numerical details

In Refs. [1] and [100], the PRM with a particle-like $h_{11/2}$ proton and a hole-like $h_{11/2}$ neutron for $\gamma = 30°$ is used to study the chiral doublet bands and the MχD respectively with identical configuration. In Ref. [67], the same system is discussed with different triaxial deformation parameters $\gamma = 30°$, $27°$, $24°$, $21°$, $18°$, and $15°$ to examine the B(M1) staggering as a fingerprint for chiral doublet bands. In this paper, the same model will be used to examine the robustness of MχD with

identical configuration with respect to the triaxiality of the nucleus. For all the PRM calculations, we employ a symmetric particle–hole configuration $\pi h_{11/2} \otimes \nu h_{11/2}^{-1}$, quadrupole deformation with $\beta = 0.25$, and moment of inertia $\mathcal{J}_0 = 30 \text{ MeV}^{-1}\hbar^2$. For the electromagnetic transition calculations, the empirical intrinsic quadrupole moment $Q_0 = (3/\sqrt{5\pi}R_0^2 Z\beta) = 3.5$ eb, gyromagnetic ratios $g_R = Z/A = 0.44$, and $g_p = 1.21$, $g_n = -0.21$ are used [61, 67, 100] in accordance with the mass region $A \sim 130$. The numerical details used here are in agreement with Ref. [67], and only β is sightly different ($\beta = 0.22$ in Ref. [67]). Thus, the discussions of bands 1 and 2 presented in Ref. [67] still hold true here, and we focus on the higher excited bands 3 and 4.

4 Results and discussion

4.1 Energy spectra

Figure 1 shows the energy spectra of the four lowest bands 1, 2, 3 and 4 calculated in the PRM when the triaxial deformation parameter γ varies from $30°$ to $15°$. The discussions about the changing of the energy spectra with respect to γ for bands 1 and 2 can be found in Ref. [67]. For $\gamma = 30°$, it is difficult to distinguish the doublet bands 1 and 2. As γ deviates from $30°$, the energy difference between the bands 1 and 2 increases.
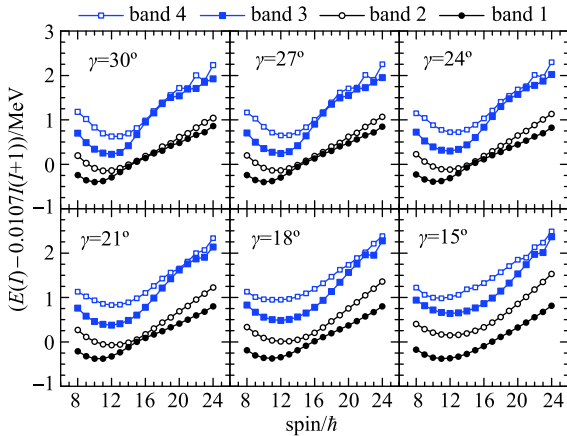

Fig. 1. (color online) The energy spectra of the four lowest bands for the configuration $\pi h_{11/2}^1 \otimes \nu h_{11/2}^{-1}$ with deformation parameter $\beta = 0.25$ and moment of inertia $\mathcal{J} = 30 \text{ MeV}^{-1}\hbar^2$ calculated by the PRM with different triaxial deformation parameters γ. The energy of a rigid-rotor has been subtracted from the total energies.

Similar behavior can also be found in doublet bands 3 and 4. For $\gamma = 30°$, analogous to bands 1 and 2, the energy of bands 3 and 4 is identical when $16\hbar \leqslant I \leqslant 19\hbar$. The energy differences between these two bands vanish, indicating that static chirality appears. In addition, the energy differences between neighboring bands at low

spin region ($8\hbar \leqslant I \leqslant 12\hbar$) are approximately the same, which may correspond to the chiral vibration [38, 66]. When γ gradually deviates from $30°$, the degeneracy at $16\hbar \leqslant I \leqslant 19\hbar$ is gradually removed. Especially when $\gamma = 15°$, the two energy differences between bands 3 and 4 is larger than 0.4 MeV, suggesting the absence of static chirality. In contrast to the static chirality, the chiral vibration remains when γ decreases.

4.2 Electromagnetic transition probabilities

Besides the small energy difference, the similarity of the electromagnetic transition probabilities and the odd–even staggering of $B(M1)$ are remarkable characteristics for chiral doublet bands [35, 36, 59, 63, 67, 100]. It has been demonstrated that for the yrast and yrare bands, the $B(M1)$ staggering is weak in the chiral vibration region, while it is strong in the static chirality region [67]. Here, we discuss the electromagnetic transition probabilities for bands 3 and 4. The calculated intra- and inter-band reduced magnetic dipole transitions probabilities $B(M1)$ and electric quadrupole transitions probabilities $B(E2)$ of bands 3 and 4 by the PRM are shown in Fig. 2 and 3 respectively with different triaxial deformation parameters γ. Notice that the intra-band transition probabilities of the doublet bands exhibit a similar tendency. The same phenomena also take place in inter-band transition probabilities. This suggests that the chiral doublet bands might remain in bands 3 and 4 when γ deviates from $30°$.

As shown in Fig. 2, for $\gamma = 30°$, when $I \leqslant 15\hbar$, the intra-band $B(M1)$ decreases gradually with spin, while the inter-band M1 transitions are forbidden. For $I > 15\hbar$, a strong staggering between bands 3 and 4 can be seen clearly, which means there is an alternative suppression between the intra- and inter- transition as spin increases. This has been demonstrated in Ref. [100]. However, as γ deviates from $30°$, two obvious changes happen. One is that the staggering becomes weaker and weaker in the high spin region; the other is that the suppression of inter-band transitions is gradually relieved in the low spin region. Compared with the first partner bands 1 and 2, for which the staggering when $\gamma = 15°$ completely disappears [67], the staggering of the second partner bands 3 and 4 still exists at the same spin interval.

Figure 3 shows the electric quadrupole transition probabilities $B(E2)$ between the second partner bands. It can be seen that for $\gamma = 30°$, when $I \leqslant 15\hbar$, the intra-band E2 transitions are forbidden, and the inter-band transitions are allowed. On the contrary, when $I > 15\hbar$, the intra-band E2 transitions are allowed, and the inter-band E2 transitions are forbidden. As γ deviates from $30°$, the probabilities of both intra- and inter-transitions for $I > 20\hbar$ are similar, which indicates that $B(E2)$ is irrelevant to γ at high spin. At low spin ($I \leqslant 20\hbar$), the

situation is reversed: the suppressed inter-band transitions are gradually allowed, yet intra-bands are gradually forbidden. Similar conclusions for bands 1 and 2 were derived in Ref. [67].
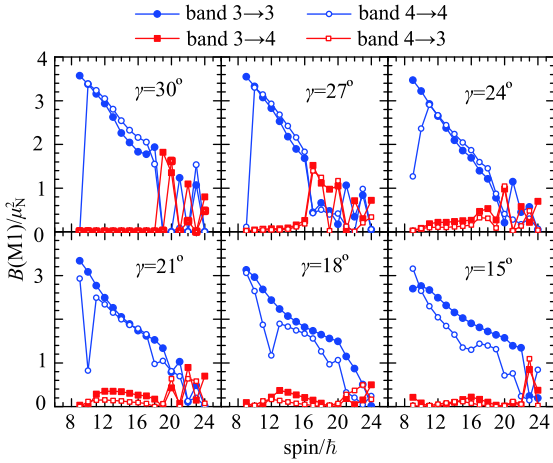

Fig. 2. (color online) The intra- (band 3 → band 3 and band 4 → band 4) and inter-band (band 3 → band 4 and band 4 → band 3) reduced magnetic dipole transition probabilities B(M1) of bands 3 and 4 calculated by the PRM with different triaxial deformation parameters γ.
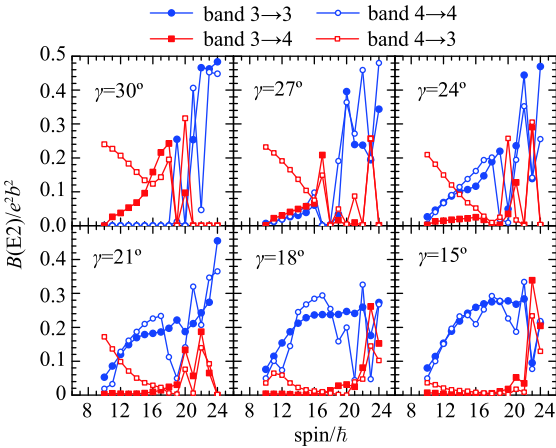

Fig. 3. (color online) The intra- (band 3 → band 3 and band 4 → band 4) and inter-band (band 3 → band 4 and band 4 → band 3) reduced electric quadrupole transition probabilities B(E2) of bands 3 and 4 calculated by the PRM with different triaxial deformation parameters γ.

Therefore, from the discussions above, it can be found that for $I > 18\hbar$, the odd–even staggering of B(M1) will lead to the staggering of B(M1)/B(E2) and B(M1)$_{\rm in}$/B(M1)$_{\rm out}$. When γ gradually decreases, the amplitude of B(M1)/B(E2) and B(M1)$_{\rm in}$/B(M1)$_{\rm out}$ staggering will decline because of the weakening of B(M1) staggering.

4.3   Angular momenta

An insight into chiral geometry will be revealed when it comes to the rms values of the angular momenta components of the core $R_k = \langle \hat{R}_k^2 \rangle^{1/2}$, the valence proton $J_{\rm pk} = \langle \hat{j}_{\rm pk}^2 \rangle^{1/2}$, and the valence neutron $J_{\rm nk} = \langle \hat{j}_{\rm nk}^2 \rangle^{1/2}$ ($k = 1, 2, 3$). The results for bands 1 and 2 have already shown in Ref. [67], where the chiral geometry for the doublet bands is discussed. The obtained results for bands 3 and 4 at triaxial deformation parameter $\gamma = 30°, 21°, 15°$ are shown in Fig. 4, in which l, i, s correspond to long, intermediate and short axes. It is shown that for both partner bands, the core angular momentum mainly aligns along the i-axis due to its largest moment of inertia. The contribution of the valence proton particle aligns mainly along the s-axis, and that of the valence neutron hole mainly aligns along the l-axis, for such orientations are favored by their interaction with the triaxial core [1]. With the total angular momentum increasing, $\boldsymbol{R}$ increases gradually, $\boldsymbol{J}_{\rm n}$ and $\boldsymbol{J}_{\rm p}$ move gradually toward the i-axis due to the Coriolis interaction, and the three angular momenta together form the chiral geometry of aplanar rotation.

It can be easily seen that when $\gamma = 30°$, the angular momenta of bands 3 and 4 are almost the same, except at the band head and $I = 20\hbar$. They have a similar orientation. However, as γ gradually deviates from 30°, this similarity gradually disappears. When $\gamma = 21°$, the differences between the partner bands become larger than those when $\gamma = 30°$, yet at $I = 20\hbar, 21\hbar, 23\hbar$, the two bands are still similar. As γ continually decreases, such as $\gamma = 15°$, the orientation of angular momenta at $20\hbar < I < 24\hbar$ of the core, valence proton and neutron are different, corresponding to the large energy difference between bands 3 and 4 shown in Fig. 1.

4.4 K-distributions

To understand the mechanism of chiral geometry better, the K-distributions, which reveal the probability distributions of the projection on three principle axes of the total angular momenta, are studied.

As discussed above, at low spin, the valence proton particle and neutron hole contribute most to the total angular momentum. Thus the angular momentum mainly lies in the s-l plane, as diagrammatically shown in Fig. 5. Due to the effect of quantal fluctuation, the total angular momentum will vibrate through the s-l plane. In this case, the chiral vibration will appear since the total angular momentum oscillates between the left-handed and right-handed systems [38, 66]. To illustrate the vibrational character of this dynamic chirality procedure, Fig. 6 shows the K-distribution along the i-axis of the four lowest energy bands for $\gamma = 30°$ at $I = 10\hbar$. The K-distribution of bands 1 and 2 have been shown in Ref. [67], where it has been pointed out that bands 1 and
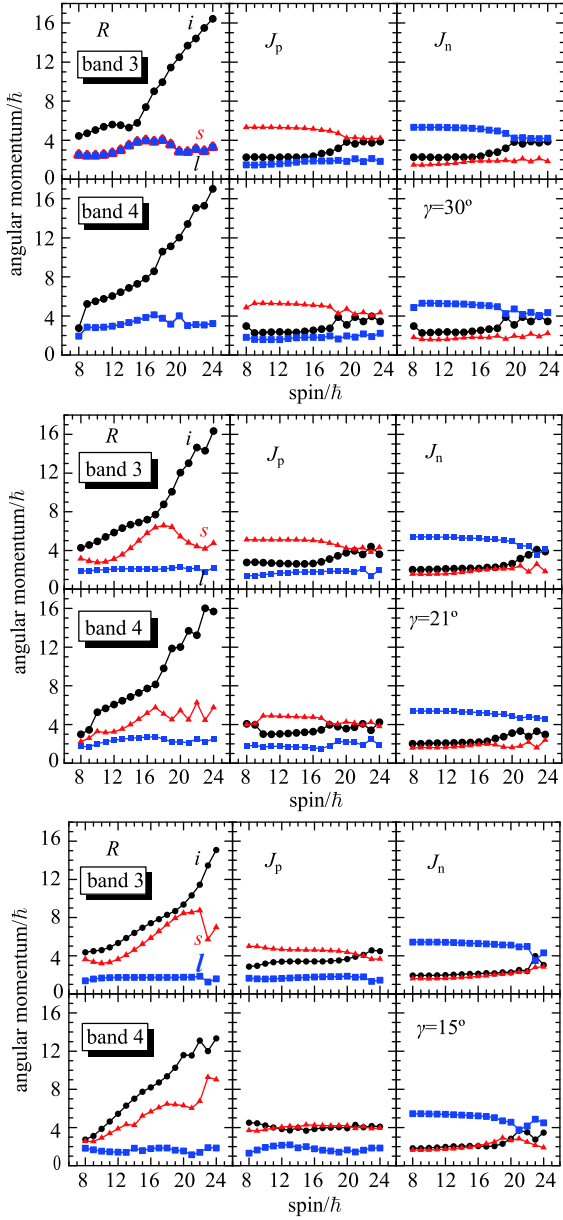
Fig. 4.   (color online) The expectation values of angular momenta of the core ($R_k = \sqrt{\langle \hat{R}_k^2 \rangle}$), the valence proton particle ($J_{pk} = \sqrt{\langle \hat{J}_{pk}^2 \rangle}$), and the valence neutron hole ($J_{nk} = \sqrt{\langle \hat{J}_{nk}^2 \rangle}$) along the intermediate (i), short (s), and long (l) axes with the triaxial deformation parameter $\gamma = 30°, 21°, 15°$.

2 correspond to the zero- and one-phonon states with symmetric and antisymmetric wave functions on the i-axis. In the same way, bands 3 and 4 represent two- and three-phonon states with symmetric and antisymmetric wave functions. The chiral vibration characteristic in the low spin region can explain the similar spacing between the neighboring bands at the beginning of the MχD as shown in Fig. 1. It is worth noting that compared to

K-distribution along the i-axis, the differences between the K-distributions along the s-and l-axes are quiet substantial (as shown in Fig. 7), which presumably indicate changes in the coupling of the quasiparticles to the triaxial core [67].
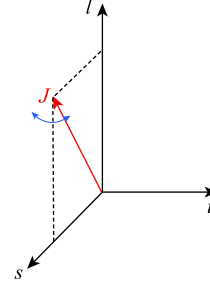

Fig. 5.   (color online) Diagrammatic sketch of chiral vibration of total angular momentum.

The obtained results for bands 3 and 4 at triaxial deformation parameter $\gamma = 30°, 21°, 15°$ are shown in Fig. 7. In the following discussions, we use K_s, K_i, and K_l to represent the distributions on the short, intermediate, and long axis respectively.
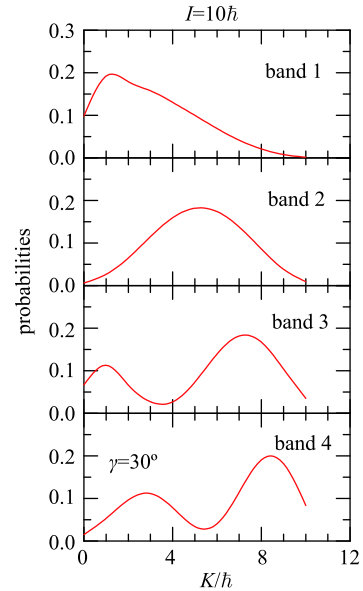

Fig. 6.   (color online) The K-distribution of four lowest bands 1, 2, 3, and 4 for $\gamma = 30°$ when $I = 10\hbar$.

For $\gamma = 30°$, in the high spin region, such as $I = 18\hbar, 22\hbar$, the K-distributions of the partner bands turn out to be similar, implying the alteration from chiral vibration to static chirality [100].

As γ decreases, e.g., $\gamma = 21°$, the K-distribution of bands 3 and 4 when $I < 20\hbar$ is similar to that when $\gamma = 30°$. But another mode of new type of chiral vibration is found when $I > 20\hbar$. The maximum K_s distribution at that interval appears near $K_s = 0$ for band 3

and band 4, which corresponds to the chiral vibration through the l-i plane.

When $\gamma = 15°$, two modes of chiral vibration remain at low and high spin, but the pure static chirality is hardly distinguishable. Thus, for spin $16\hbar < I < 20\hbar$, chiral vibration is mixed with static chirality, which may characterize energy spectra by the removal of degeneracy at $16\hbar < I < 20\hbar$.
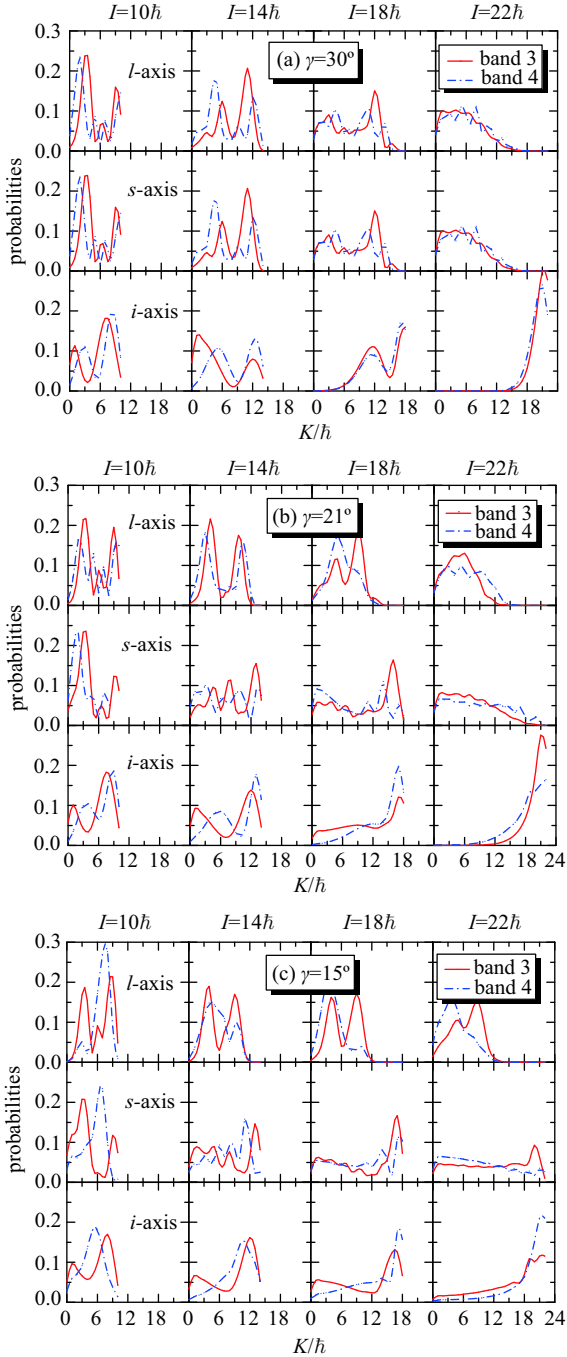

Fig. 7. (color online) Probability distributions of the projection of total angular momenta of bands 3 and 4 along the intermediate, short, and long axes when the parameter $\gamma = 30°, 21°, 15°$.

4.5   Energy spectra for higher excited states

The discussion above gives the results of the physical observables and chiral geometry of the MχD with identical configuration for different triaxial parameters γ with $\pi h_{11/2} \otimes \nu h_{11/2}^{-1}$. It has been shown that the chirality still remains not only in the yrast and yrare bands, but also in the two higher excited bands when γ deviates from $30°$. Further consideration of higher excited bands seems interesting. In Refs. [89, 100], the energy spectra of higher excited bands 5 and 6 have been shown at $\gamma = 30°$. It is found that bands 5 and 6 might also be a pair of chiral doublet bands. In Fig. 8, the energy states as well as their excitation energies with respect to the yrast states obtained by PRM with triaxial deformation parameters $\gamma = 30°$ are shown as functions of spin. For each spin, the lowest twenty states are shown. It can be seen that in high excited bands, whose excitation energies are larger than 2.0 MeV, the situation turns out to be complex. The level density is rather high, and neighboring bands are too close to be distinguished. Thus it would be very difficult, if not impossible, to select the chiral doublet bands [100]. In fact, these states would fall into the regime of quasi-continuum spectra and the strong interactions between them evoke the emergence of rotation damping [104, 105]. This complexity can be explained by the PRM Hamiltonian (1), where the single particles, the rotor, and their coupling Hamiltonian are involved. If the single particles were not considered, it would turn into a triaxial wobbling rotor Hamiltonian [106]. In the spin region ($8 \sim 20\hbar$) discussed above, the wobbling rotor has a low angular momentum ($\sim 10\hbar$), which corresponds to a complicated wobbling energy spectrum [106–109]. With the coupling of the single particles, the occupation of proton and neutron at different orbitals further complicates the wobbling energy spectra of the triaxial rotor.

In addition, the energy spectra of higher excited states with triaxiality parameters smaller than $\gamma = 30°$ are also examined. We note that the triaxial deformation has a larger influence on the low lying states than on high ones. When the triaxial deformation parameter varies from $30°$ to $15°$, the complexity of the high energy states still remains. More effort needs to be invested in investigating the higher excited states.

5   Summary

In summary, the chiral geometry of the MχD with identical configuration has been discussed for different triaxial deformation parameters γ with $\pi h_{11/2} \otimes \nu h_{11/2}^{-1}$ in the particle rotor model. The energy spectra, electromagnetic transition probabilities $B(M1)$ and $B(E2)$, angular momenta, and K-distributions have been studied. The calculated results strongly suggest the chirality still remains in not only the yrast and yrare bands but
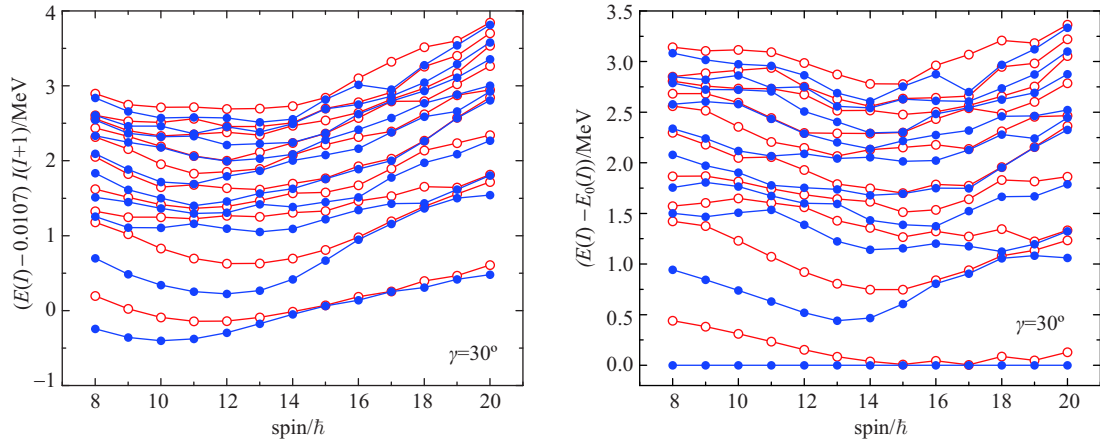
Fig. 8.   (color online) The energy states and their excitation energies with respect to the yrast state obtained by the PRM with triaxial deformation parameters $\gamma = 30°$. For each spin, the lowest twenty states are shown.

also the two higher excited bands when γ deviates from $30°$. The chiral geometry relies on γ, for the chiral vibration and static chirality exist in different spin intervals when γ changes. In addition, the chiral geometry of the higher energy partner bands is not as obvious as that of those with the lowest energy.

References

1 S. Frauendorf and J. Meng, Nucl. Phys. A, **617**: 131 (1997)
2 K. Starosta, T. Koike, C. J. Chiara et al, Phys. Rev. Lett., **86**: 971 (2001)
3 S. Y. Wang, B. Qi, L. Liu et al, Phys. Lett. B, **703**: 40 (2011)
4 C. Vaman, D. B. Fossan, T. Koike, K. Starosta, I. Y. Lee, and A. O. Macchiavelli, Phys. Rev. Lett., **92**: 032501 (2004)
5 P. Joshi, D. G. Jenkins, P. M. Raddon et al, Phys. Lett. B, **595**: 135 (2004)
6 J. A. Alcántara-Núñez, J. R. B. Oliveira, E. W. Cybulska et al, Phys. Rev. C, **69**: 024317 (2004)
7 J. Timár, P. Joshi, K. Starosta et al, Phys. Lett. B, **598**: 178 (2004)
8 Y. X. Luo, S. C. Wu, J. Gilat et al, Phys. Rev. C, **69**: 024315 (2004)
9 P. Joshi, A. R. Wilkinson, T. Koike et al, Eur. Phys. J. A, **24**: 23 (2005)
10 S. J. Zhu, J. H. Hamilton, A. V. Ramayya et al, Eur. Phys. J. A, **25**: 459 (2005)
11 J. Timár, C. Vaman, K. Starosta et al, Phys. Rev. C, **73**: 011301 (2006)
12 P. Joshi, M. P. Carpenter, D. B. Fossan et al, Phys. Rev. Lett., **98**: 102501 (2007)
13 J. Timár, T. Koike, N. Pietralla et al, Phys. Rev. C, **76**: 024307 (2007)
14 T. Suzuki, G. Rainovski, T. Koike et al, Phys. Rev. C, **78**: 031302 (2008)
15 Y. X. Luo, S. J. Zhu, J. H. Hamilton et al, Phys. Lett. B, **670**: 307 (2009)
16 J. Sethi, R. Palit, S. Saha et al, Phys. Lett. B, **725**: 85 (2013)
17 D. Tonev, M. S. Yavahchova, N. Goutev et al, Phys. Rev. Lett., **112**: 052501 (2014)
18 E. O. Lieder, R. M. Lieder, R. A. Bark et al, Phys. Rev. Lett., **112**: 202502 (2014)
19 N. Rather, P. Datta, S. Chattopadhyay et al, Phys. Rev. Lett., **112**: 202503 (2014)

20 D. J. Hartley, L. L. Riedinger, M. A. Riley et al, Phys. Rev. C, **64**: 031304 (2001)
21 A. A. Hecht, C. W. Beausang, K. E. Zyromski et al, Phys. Rev. C, **63**: 051302 (2001)
22 T. Koike, K. Starosta, C. J. Chiara, D. B. Fossan and D. R. LaFosse, Phys. Rev. C, **63**: 061304 (2001)
23 R. A. Bark, A. M. Baxter, A. P. Byrne, G. D. Dracoulis, T. Kibedi, T. R. McGoram, and S. M. Mullins, Nucl. Phys. A, **691**: 577 (2001)
24 K. Starosta, C. J. Chiara, D. B. Fossan, T. Koike, T. T. S. Kuo, D. R. LaFosse, S. G. Rohozinski, Ch. Droste, T. Morek and J. Srebrny, Phys. Rev. C, **65**: 044328 (2002)
25 E. Mergel, C. M. Petrache, G. Lo Bianco et al, Eur. Phys. J. A, **15**: 417 (2002)
26 X. F. Li, Y. J. Ma, Y. Z. Liu et al, Chin. Phys. Lett., **19**: 1779 (2002)
27 S. Zhu, U. Garg, B. K. Nayak et al, Phys. Rev. Lett., **91**: 132501 (2003)
28 A. A. Hecht, C. W. Beausang, H. Amro et al, Phys. Rev. C, **68**: 054310 (2003)
29 T. Koike, K. Starosta, C. J. Chiara, D. B. Fossan, and D. R. LaFosse, Phys. Rev. C, **67**: 044319 (2003)
30 G. Rainovski, E. S. Paul, H. J. Chantler et al, Phys. Rev. C, **68**: 024318 (2003)
31 S. P. Roberts, T. Ahn, K. Starosta, T. Koike, C. J. Chiara and C. Vaman, Phys. Rev. C, **67**: 057301 (2003)
32 G. Rainovski, E. S. Paul, H. J. Chantler et al, J. Phys. G: Nucl. Part. Phys., **29**: 2763 (2003)
33 A. J. Simons, P. Joshi, D. G. Jenkins et al, J. Phys. G: Nucl. Part. Phys., **31**: 541 (2005)
34 E. Grodner, J. Srebrny, A. A. Pasternak et al, Phys. Rev. Lett., **97**: 172501 (2006)
35 C. M. Petrache, G. B. Hagemann, I. Hamamoto, and K. Starosta, Phys. Rev. Lett., **96**: 112502 (2006)
36 D. Tonev, G. de Angelis, P. Petkov et al, Phys. Rev. Lett., **96**: 052501 (2006)
37 S. Y. Wang, Y. Z. Liu, I. Komatsubara, Y. J. Ma, and Y. H. Zhang, Phys. Rev. C, **74**: 017302 (2006)

38 S. Mukhopadhyay, D. Almehed, U. Garg et al, Phys. Rev. Lett., **99**: 172501 (2007)

39 D. Tonev, G. de Angelis, S. Brant et al, Phys. Rev. C, **76**: 044313 (2007)

40 Y. X. Zhao, I. Komatsubara, Y. J. Ma , Y. H. Zhang, S. Y. Wang, Y. Z. Liu, and K. Furuno, Chin. Phys. Lett., **26**: 082301 (2009)

41 E. Grodner, I. Sankowska, T. Morek et al, Phys. Lett. B, **703**: 46 (2011)

42 J. Timár, K. Starosta, I. Kuti et al, Phys. Rev. C, **84**: 044302 (2011)

43 K. Y. Ma, J. B. Lu, D. Yang, H. D. Wang, Y. Z. Liu, X. G. Wu, Y. Zheng, and C. Y. He, Phys. Rev. C, **85**: 037301 (2012)

44 C. M. Petrache, S. Frauendorf, M. Matsuzaki et al, Phys. Rev. C, **86**: 044321 (2012)

45 I. Kuti, J. Timar, D. Sohler et al, Phys. Rev. C, **87**: 044323 (2013)

46 D. L. Balabanski, M. Danchev, D. J. Hartley et al, Phys. Rev. C, **70**: 044305 (2004)

47 E. A. Lawrie, P. A. Vymers, J. J. Lawrie et al, Phys. Rev. C, **78**: 021305 (2008)

48 E. A. Lawrie, P. A. Vymers, Ch. Vieu et al, Eur. Phys. J. A, **45**: 39 (2010)

49 P. L. Masiteng, E. A. Lawrie, T. M. Ramashidzha et al, Phys. Lett. B, **719**: 83 (2013)

50 P. L. Masiteng, E. A. Lawrie, T. M. Ramashidzha et al, Eur. Phys. J. A, **50**: 119 (2014)

51 J. Meng, B. Qi, S. Q. Zhang, and S. Y. Wang, Mod. Phys. Lett. A, **23**: 2560 (2008)

52 B. Qi, *Static and dynamic chirality in atomic nuclei*, PhD thesis, (Peking University, 2009)

53 J. Meng and S. Q. Zhang, J. Phys. G: Nucl. Part. Phys., **37**: 064025 (2010)

54 J. Meng, Q. B. Chen, and S. Q. Zhang, Int. J. Mod. Phys. E, **23**: 1430016 (2014)

55 R. A. Bark, E. O. Lieder, R. M. Lieder et al, Int. J. Mod. Phys. E, **23**: 1461001 (2014)

56 Q. B. Chen, *Collective Hamiltonian for nuclear chiral and wobbling modes*, PhD thesis (Peking University, 2015)

57 J. Peng, J. Meng, and S. Q. Zhang, Phys. Rev. C, **68**: 044324 (2003)

58 J. Peng, J. Meng, and S. Q. Zhang, Chin. Phys. Lett., **20**: 1223 (2003)

59 T. Koike, K. Starosta, and I. Hamamoto, Phys. Rev. Lett., **93**: 172502 (2004)

60 S. Q. Zhang, B. Qi, S. Y. Wang and J. Meng, Phys. Rev. C, **75**: 044307 (2007)

61 S. Y. Wang, S. Q. Zhang, B. Qi, and J. Meng, Phys. Rev. C, **75**: 024309 (2007)

62 K. Higashiyama and N. Yoshinaga, Eur. Phys. J. A, **33**: 355 (2007)

63 S. Y. Wang, S. Q. Zhang, B. Qi, and J. Meng, Chin. Phys. Lett., **24**: 664 (2007)

64 S. Y. Wang, S. Q. Zhang, B. Qi, J. Peng, J. M. Yao, and J. Meng, Phys. Rev. C, **77**: 034314 (2008)

65 S. Y. Wang, S. Q. Zhang, B. Qi, and J. Meng, Chin. Phys. C, **32**: 138 (2008)

66 B. Qi, S .Q. Zhang, J. Meng, S. Y. Wang, and S. Frauendorf, Phys. Lett. B, **675**: 175 (2009)

67 B. Qi, S. Q. Zhang, S. Y. Wang, J. M. Yao, and J. Meng, Phys. Rev. C, **79**: 041302(R) (2009)

68 S. Y. Wang, B. Qi, and S. Q. Zhang, Chin. Phys. Lett., **26**: 052102 (2009)

69 S. Y. Wang, S. Q. Zhang, B. Qi, and J. Meng, Chin. Phys. C, **33**: 37 (2009)

70 E. A. Lawrie and O. Shirinda, Phys. Lett. B, **689**: 66 (2010)

71 S. G. Rohozinski, L. Prochniak, K. Starosta, and Ch. Droste, Eur. Phys. J. A, **47**: 90 (2011)

72 S. C. Rohozinski, L. Prochniak, Ch. Droste, and K. Starosta, Int. J. Mod. Phys. E, **20**: 364 (2011)

73 B. Qi, S. Q. Zhang, S. Y. Wang, J. Meng, and T. Koike, Phys. Rev. C, **83**: 034303 (2011)

74 B. Qi, S. Y. Wang, and S. Q. Zhang, Chin. Phys. Lett., **28**: 122101 (2011)

75 O. Shirinda and E. A. Lawrie, Eur. Phys. J. A, **48**: 118 (2012)

76 S. Y. Wang, B. Qi, and D. P. Sun, Phys. Rev. C, **82**: 027303 (2010)

77 V. I. Dimitrov, S. Frauendorf, and F. Dönau, Phys. Rev. Lett., **84**: 5732 (2000)

78 P. Olbratowski, J. Dobaczewski, J. Dudek, and W. Płóciennik, Phys. Rev. Lett., **93**: 052501 (2004)

79 P. Olbratowski, J. Dobaczewski, and J. Dudek, Phys. Rev. C, **73**: 054308 (2006)

80 D. Almehed, F. Dönau, and S. Frauendorf, Phys. Rev. C, **83**: 054308 (2011)

81 S. Brant, D. Vretenar, and A. Ventura, Phys. Rev. C, **69**: 017304 (2004)

82 S. Brant, D. Tonev, G. de Angelis, and A. Ventura, Phys. Rev. C, **78**: 034301 (2008)

83 S. Brant and C. M. Petrache, Phys. Rev. C, **79**: 054326 (2009)

84 H. G. Ganev and S. Brant, Phys. Rev. C, **82**: 034328 (2010)

85 K. Higashiyama, N. Yoshinaga, and K. Tanabe, Phys. Rev. C, **72**: 024315 (2005)

86 N. Yoshinaga and K. Higashiyama, J. Phys. G: Nucl. Part. Phys., **31**: S1455 (2005)

87 N. Yoshinaga and K. Higashiyama, Eur. Phys. J. A, **30**: 343 (2006)

88 G. H. Bhat, J. A. Sheikh, W. A. Dar, S. Jehangir, R. Palit, and P. A. Ganai, Phys. Lett. B, **738**: 218 (2014)

89 Q. B. Chen, S. Q. Zhang, P. W. Zhao, R. V. Jolos, and J. Meng, Phys. Rev. C, **87**: 024314 (2013)

90 P. Ring, Prog. Part. Nucl. Phys., **37**: 193–263 (1996)

91 D. Vretenar, A.V. Afanasjev, G.A. Lalazissis, and P. Ring, Phys. Rep., **409**: 101–259 (2005)

92 J. Meng, H. Toki, S.G. Zhou, S.Q. Zhang, W.H. Long, and L.S. Geng, Prog. Part. Nucl. Phys., **57**: 470–563 (2006)

93 J. Meng, J. Peng, S. Q. Zhang, and S.-G. Zhou, Phys. Rev. C, **73**: 037303 (2006)

94 J. Peng, H. Sagawa, S. Q. Zhang, J. M. Yao, Y. Zhang, and J. Meng, Phys. Rev. C, **77**: 024309 (2008)

95 J. M. Yao, B. Qi, S. Q. Zhang, J. Peng, S. Y. Wang, and J. Meng, Phys. Rev. C, **79**: 067302 (2009)

96 J. Li, S. Q. Zhang, and J. Meng, Phys. Rev. C, **83**: 037301 (2011)

97 A. D. Ayangeakaa, U. Garg, M. D. Anthony et al, Phys. Rev. Lett., **110**: 172504 (2013)

98 B. Qi, H. Jia, N. B. Zhang, C. Liu, and S. Y. Wang, Phys. Rev. C, **88**: 027302 (2013)

99 Ch. Droste, S. G. Rohozinski, K. Starosta, L. Prochniak, and E. Grodner, Eur. Phys. J. A, **42**: 79 (2009)

100 Q. B. Chen, J. M. Yao, S. Q. Zhang, and B. Qi, Phys. Rev. C, **82**: 067302 (2010)

101 I. Hamamoto, Phys. Rev. C, **88**: 024327 (2013)

102 I. Kuti, Q. B. Chen, J. Timár et al, Phys. Rev. Lett., **113**: 032501 (2014)

103 P. Ring and P. Schuck,   *The nuclear many body problem* (Berlin: Springer Verlag, 1980)

104 T. Døssing, B. Herskind, S. Leoni, A. Bracco, R.A. Broglia, M. Matsuo, and E. Vigezzi, Phys. Rep., **268**: 1 (1996)

105 A. Bracco and S. Leoni, Rep. Prog. Phys., **65**: 299 (2002)

106 A. Bohr and B. R. Mottelson, *Nuclear structure*, volume II. (New York: Benjamin, 1975)

107 S. Frauendorf and F. Dönau, Phys. Rev. C, **89**: 014322 (2014)

108 Q. B. Chen, S. Q. Zhang, P. W. Zhao, and J. Meng, Phys. Rev. C, **90**: 044306 (2014)

109 W. X. Shi and Q. B. Chen, Chin. Phys. C, **39**: 054105 (2015)